Author(s): Hinkkanen, Marko & Repo, Anna-Kaisa & Ranta, Mikaela & Luomi, Jorma

Title: Small-Signal Modeling of Mutual Saturation in Induction Machines

Year: 2010

Version: Post print

Please cite the original version:

Hinkkanen, Marko & Repo, Anna-Kaisa & Ranta, Mikaela & Luomi, Jorma. 2010. Small-Signal Modeling of Mutual Saturation in Induction Machines. IEEE Transactions on Industry Applications. Volume 46, Issue 3. 965-973. ISSN 0093-9994 (printed). DOI: 10.1109/tia.2010.2046290.

Small-Signal Modeling of Mutual Saturation in Induction Machines

Marko Hinkkanen, *Member, IEEE,* Anna-Kaisa Repo, Mikaela Ranta, and Jorma Luomi, *Member, IEEE*

***Abstract*—A small-signal model is derived for saturated induction machines. Inductances are allowed to saturate as a function of their own current (or flux), and the mutual saturation effect originating mainly from skewed or closed rotor slots is also included in the model. The model fulfills the reciprocity conditions, and it can be applied to parameter identification and to the analysis and development of flux angle estimation methods. As application examples, the parameters of a 2.2-kW induction machine were identified using the data obtained from time-stepping finite-element analysis and locked-rotor measurements. The proposed model fits well to the data, and the fitted parameters are physically reasonable.**

***Index Terms*—Closed slots, induction motors, magnetic saturation, motor models, reciprocity, rotor skew, signal injection.**

I. Introduction

Induction machines are usually magnetically saturated in the rated operating point. Conventionally, the main flux is assumed to saturate only as a function of the magnetizing current. However, it has been observed that the main flux may depend significantly on the load [1], [2]. This mutual saturation effect originates mainly from skewed and closed rotor slots [3], which are used in the majority of small machines.

Magnetic saturation affects the transient behavior of the machine, but the effects of saturation are not well known. For example, the dynamical effects of saturation are usually ignored in parameter identification methods that rely on transient behaviour [4]. Consequently, incremental parameters may be unintentionally identified in practical saturated conditions instead of the expected steady-state parameters. Other examples are various flux estimation methods based on saturation-induced spatial anisotropies, e.g. [5], [6]. Conventionally, heuristic high-frequency small-signal models are applied in the analysis of these methods. Saturation-induced anisotropies depend on the load and flux level, and they are generally not fixed in position relative to any flux component [7].

The small-signal impedance of a saturated machine depends on the direction of the excitation signal [8]; this phenomenon has been modeled assuming that the main flux depends only on the magnetizing current [9], [10]. However, the saturation phenomena specific to machines with closed or skewed rotor slots are more complicated, and this assumption should be relaxed.

It is common practice to consider the losses dissipated in the magnetic circuit separately, and to use lossless inductors to model the magnetic circuit as in Fig. 1. The saturable magnetic circuit should fulfill the reciprocity conditions [11], [12] since otherwise the magnetic circuit may unintentionally behave as an energy source or sink. In other words, the energy stored in the magnetic circuit should be independent of the integration path. When relaxing the assumptions relating to the saturation, these conditions have to be taken into account.

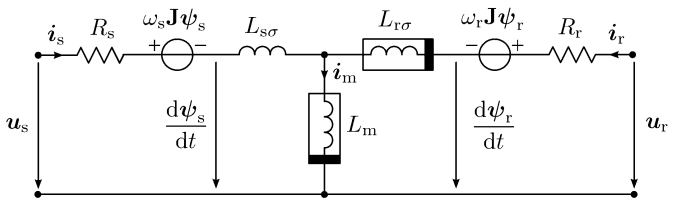

Fig. 1. Dynamic T model of an induction motor in coordinates rotating at ω_s. The angular slip frequency is $\omega_\mathrm{r} = \omega_\mathrm{s} - \omega_\mathrm{m}$, where ω_m is the angular speed of the rotor.

This paper presents a small-signal model suitable for saturated induction machines that may have closed or skewed rotor slots. Each inductance is allowed to saturate as a function of its own current (or flux), and the mutual saturation effect is also included in the model. The proposed model fulfills the reciprocity conditions. As an example, the model is applied to parameter identification of a 2.2-kW induction machine. The identification data is produced using time-stepping finite-element analysis (FEA) [13] and locked-rotor measurements. Voltage pulses [14] and pulsating voltage-signal injection are used as excitation signals.

II. Machine Model

Vectors will be denoted by boldface lowercase letters and matrices by boldface uppercase letters. The matrix transpose will be marked with the superscript T. The identity matrix, the orthogonal rotation matrix, and the zero matrix are

$$\mathbf{I} = \begin{bmatrix} 1 & 0 \\ 0 & 1 \end{bmatrix}, \quad \mathbf{J} = \begin{bmatrix} 0 & -1 \\ 1 & 0 \end{bmatrix}, \quad \mathbf{O} = \begin{bmatrix} 0 & 0 \\ 0 & 0 \end{bmatrix} \tag{1}$$

respectively. Incremental inductances will be marked with the subscript t.

A. Large-Signal T Model

In a general coordinate system rotating at angular speed ω_s, the voltage equations of the induction machine are

$$\frac{\mathrm{d}\boldsymbol{\psi}_\mathrm{s}}{\mathrm{d}t} = \boldsymbol{u}_\mathrm{s} - R_\mathrm{s}\boldsymbol{i}_\mathrm{s} - \omega_\mathrm{s}\mathbf{J}\boldsymbol{\psi}_\mathrm{s} \tag{2a}$$

$$\frac{\mathrm{d}\boldsymbol{\psi}_\mathrm{r}}{\mathrm{d}t} = \boldsymbol{u}_\mathrm{r} - R_\mathrm{r}\boldsymbol{i}_\mathrm{r} - (\omega_\mathrm{s} - \omega_\mathrm{m})\,\mathbf{J}\boldsymbol{\psi}_\mathrm{r} \tag{2b}$$

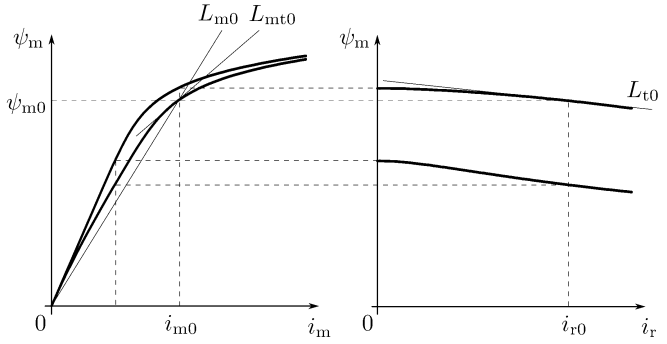

Fig. 2. Typical saturation characteristics of the main flux $\psi_{\mathrm{m}}(i_{\mathrm{m}}, i_{\mathrm{r}})$. On the left-hand side, the main flux is shown as a function of the magnetizing current i_{m}: the upper curve corresponds to no-load operation (rotor current $i_{\mathrm{r}} = 0$) and the lower curve corresponds to operation under load ($i_{\mathrm{r}} = i_{\mathrm{r0}}$). On the right-hand side, the main flux is shown as a function of the rotor current at two different values of the magnetizing current ($i_{\mathrm{m}} = 0.5 \cdot i_{\mathrm{m0}}$ and $i_{\mathrm{m}} = i_{\mathrm{m0}}$). Incremental inductances $L_{\mathrm{mt0}} = (\partial\psi_{\mathrm{m}}/\partial i_{\mathrm{m}})_0$ and $L_{\mathrm{t0}} = (\partial\psi_{\mathrm{m}}/\partial i_{\mathrm{r}})_0$, and the steady-state magnetizing inductance $L_{\mathrm{m0}} = \psi_{\mathrm{m0}}/i_{\mathrm{m0}}$ are shown in the operating point $\psi_{\mathrm{m0}} = \psi_{\mathrm{m}}(i_{\mathrm{m0}}, i_{\mathrm{r0}})$.

where $\boldsymbol{u}_{\mathrm{s}} = [u_{\mathrm{sd}}, u_{\mathrm{sq}}]^{\mathrm{T}}$ is the stator voltage vector, $\boldsymbol{i}_{\mathrm{s}} = [i_{\mathrm{sd}}, i_{\mathrm{sq}}]^{\mathrm{T}}$ the stator current vector, and R_{s} the stator resistance. The rotor resistance is R_{r}, the rotor voltage vector $\boldsymbol{u}_{\mathrm{r}}$, the rotor current vector $\boldsymbol{i}_{\mathrm{r}}$, and the electrical angular speed of the rotor ω_{m}.

The stator and rotor flux linkage vectors are

$$\boldsymbol{\psi}_{\mathrm{s}} = L_{\mathrm{s}}\boldsymbol{i}_{\mathrm{s}} + L_{\mathrm{m}}\boldsymbol{i}_{\mathrm{r}} \tag{3a}$$

$$\boldsymbol{\psi}_{\mathrm{r}} = L_{\mathrm{m}}\boldsymbol{i}_{\mathrm{s}} + L_{\mathrm{r}}\boldsymbol{i}_{\mathrm{r}} \tag{3b}$$

respectively, where L_{m} is the magnetizing inductance.[1] The stator and rotor inductances are defined by $L_{\mathrm{s}} = L_{\mathrm{m}} + L_{\mathrm{s}\sigma}$ and $L_{\mathrm{r}} = L_{\mathrm{m}} + L_{\mathrm{r}\sigma}$, respectively, where $L_{\mathrm{s}\sigma}$ and $L_{\mathrm{r}\sigma}$ are the stator and rotor leakage inductances, respectively. The T-equivalent flux linkage model corresponding to (3) is included in Fig. 1. The stator and rotor leakage fluxes are $\boldsymbol{\psi}_{\mathrm{s}\sigma} = L_{\mathrm{s}\sigma}\boldsymbol{i}_{\mathrm{s}}$ and $\boldsymbol{\psi}_{\mathrm{r}\sigma} = L_{\mathrm{r}\sigma}\boldsymbol{i}_{\mathrm{r}}$, respectively, and the main flux is $\boldsymbol{\psi}_{\mathrm{m}} = L_{\mathrm{m}}\boldsymbol{i}_{\mathrm{m}}$, where $\boldsymbol{i}_{\mathrm{m}} = \boldsymbol{i}_{\mathrm{s}} + \boldsymbol{i}_{\mathrm{r}}$ is the magnetizing current. All inductances are allowed to depend on the currents (or the fluxes), and they are assumed to be lossless.

B. Power Balance

For per-unit quantities, the power balance is obtained from (2) as

$$\boldsymbol{i}_{\mathrm{s}}^{\mathrm{T}}\boldsymbol{u}_{\mathrm{s}} + \boldsymbol{i}_{\mathrm{r}}^{\mathrm{T}}\boldsymbol{u}_{\mathrm{r}} = R_{\mathrm{s}}i_{\mathrm{s}}^2 + R_{\mathrm{r}}i_{\mathrm{r}}^2 + \frac{\mathrm{d}W_{\mathrm{f}}}{\mathrm{d}t} + T_{\mathrm{e}}\omega_{\mathrm{m}} \tag{4}$$

where $i_{\mathrm{s}} = \|\boldsymbol{i}_{\mathrm{s}}\|$ and the magnitudes of other vectors are denoted similarly. The electromagnetic torque is

$$T_{\mathrm{e}} = \boldsymbol{\psi}_{\mathrm{r}}^{\mathrm{T}}\mathbf{J}\boldsymbol{i}_{\mathrm{r}} = \boldsymbol{i}_{\mathrm{s}}^{\mathrm{T}}\mathbf{J}\boldsymbol{\psi}_{\mathrm{s}} \tag{5}$$

[1]Considering the stator flux $\boldsymbol{\psi}_{\mathrm{s}}$ and the rotor flux $\boldsymbol{\psi}_{\mathrm{r}}$ as state variables, the state-space representation of the saturated machine can be formed by substituting the stator and rotor currents solved from the flux equations (3) in the voltage equations (2).

and the rate of change of the magnetic energy is

$$\begin{aligned}\frac{\mathrm{d}W_{\mathrm{f}}}{\mathrm{d}t} &= \boldsymbol{i}_{\mathrm{s}}^{\mathrm{T}}\frac{\mathrm{d}\boldsymbol{\psi}_{\mathrm{s}}}{\mathrm{d}t} + \boldsymbol{i}_{\mathrm{r}}^{\mathrm{T}}\frac{\mathrm{d}\boldsymbol{\psi}_{\mathrm{r}}}{\mathrm{d}t} \\ &= i_{\mathrm{s}}\frac{\mathrm{d}\psi_{\mathrm{s}\sigma}}{\mathrm{d}t} + i_{\mathrm{m}}\frac{\mathrm{d}\psi_{\mathrm{m}}}{\mathrm{d}t} + i_{\mathrm{r}}\frac{\mathrm{d}\psi_{\mathrm{r}\sigma}}{\mathrm{d}t}\end{aligned} \tag{6}$$

The last form is obtained by assuming the flux vectors to be parallel with the corresponding current vectors in accordance with Fig. 1, while the inductances may be functions of the currents or fluxes. Based on (6), the incremental inductances should fulfill the reciprocity conditions [12]:

$$\frac{\partial\psi_{\mathrm{s}\sigma}}{\partial i_{\mathrm{m}}} = \frac{\partial\psi_{\mathrm{m}}}{\partial i_{\mathrm{s}}}, \quad \frac{\partial\psi_{\mathrm{m}}}{\partial i_{\mathrm{r}}} = \frac{\partial\psi_{\mathrm{r}\sigma}}{\partial i_{\mathrm{m}}}, \quad \frac{\partial\psi_{\mathrm{r}\sigma}}{\partial i_{\mathrm{s}}} = \frac{\partial\psi_{\mathrm{s}\sigma}}{\partial i_{\mathrm{r}}} \tag{7}$$

The reciprocity conditions are given in a more general form in Appendix A.

C. Assumptions on Magnetic Saturation

In the following, $L_{\mathrm{s}\sigma}$ is assumed constant for simplicity, but L_{m} and $L_{\mathrm{r}\sigma}$ are functions of two currents:

$$L_{\mathrm{m}}(i_{\mathrm{m}}, i_{\mathrm{r}}) = \frac{\psi_{\mathrm{m}}(i_{\mathrm{m}}, i_{\mathrm{r}})}{i_{\mathrm{m}}}, \quad L_{\mathrm{r}\sigma}(i_{\mathrm{m}}, i_{\mathrm{r}}) = \frac{\psi_{\mathrm{r}\sigma}(i_{\mathrm{m}}, i_{\mathrm{r}})}{i_{\mathrm{r}}} \tag{8}$$

(cf. illustration in Fig. 2 relating to L_{m}). The following incremental inductances fulfilling (7) are defined:

$$L_{\mathrm{mt}} = \frac{\partial\psi_{\mathrm{m}}}{\partial i_{\mathrm{m}}}; \quad L_{\mathrm{r}\sigma\mathrm{t}} = \frac{\partial\psi_{\mathrm{r}\sigma}}{\partial i_{\mathrm{r}}}; \quad L_{\mathrm{t}} = \frac{\partial\psi_{\mathrm{m}}}{\partial i_{\mathrm{r}}} = \frac{\partial\psi_{\mathrm{r}\sigma}}{\partial i_{\mathrm{m}}} \tag{9}$$

Assuming the magnetizing current magnitude i_{m} constant, the magnitude ψ_{m} of the main flux decreases as the magnitude i_{r} of the rotor current increases. Hence, the incremental mutual inductance L_{t} is negative. If needed, the saturation of $L_{\mathrm{s}\sigma}$ could be easily taken into account.

III. Linearized Model

A. Preliminaries

In the following, tildes refer to the deviation about the operating point and operating-point quantities are marked with the subscript 0, e.g., $\tilde{\boldsymbol{u}}_{\mathrm{s}} = \boldsymbol{u}_{\mathrm{s}} - \boldsymbol{u}_{\mathrm{s0}}$. Synchronous coordinates rotating at constant angular speed ω_{s0} are considered. The linearized voltage equations are

$$\frac{\mathrm{d}\tilde{\boldsymbol{\psi}}_{\mathrm{s}}}{\mathrm{d}t} = \tilde{\boldsymbol{u}}_{\mathrm{s}} - R_{\mathrm{s}}\tilde{\boldsymbol{i}}_{\mathrm{s}} - \omega_{\mathrm{s0}}\mathbf{J}\tilde{\boldsymbol{\psi}}_{\mathrm{s}} \tag{10a}$$

$$\frac{\mathrm{d}\tilde{\boldsymbol{\psi}}_{\mathrm{r}}}{\mathrm{d}t} = \tilde{\boldsymbol{u}}_{\mathrm{r}} - R_{\mathrm{r}}\tilde{\boldsymbol{i}}_{\mathrm{r}} - \omega_{\mathrm{r0}}\mathbf{J}\tilde{\boldsymbol{\psi}}_{\mathrm{r}} + \mathbf{J}\boldsymbol{\psi}_{\mathrm{r0}}\tilde{\omega}_{\mathrm{m}} \tag{10b}$$

where the operating-point angular slip frequency is $\omega_{\mathrm{r0}} = \omega_{\mathrm{s0}} - \omega_{\mathrm{m0}}$. The deviations of the stator and rotor fluxes are

$$\tilde{\boldsymbol{\psi}}_{\mathrm{s}} = L_{\mathrm{s0}}\tilde{\boldsymbol{i}}_{\mathrm{s}} + L_{\mathrm{m0}}\tilde{\boldsymbol{i}}_{\mathrm{r}} + \boldsymbol{i}_{\mathrm{m0}}\tilde{L}_{\mathrm{m}} \tag{11a}$$

$$\tilde{\boldsymbol{\psi}}_{\mathrm{r}} = L_{\mathrm{m0}}\tilde{\boldsymbol{i}}_{\mathrm{s}} + L_{\mathrm{r0}}\tilde{\boldsymbol{i}}_{\mathrm{r}} + \boldsymbol{i}_{\mathrm{m0}}\tilde{L}_{\mathrm{m}} + \boldsymbol{i}_{\mathrm{r0}}\tilde{L}_{\mathrm{r}\sigma} \tag{11b}$$

respectively. The linearized torque expression is

$$\tilde{T}_{\mathrm{e}} = \boldsymbol{\psi}_{\mathrm{r0}}^{\mathrm{T}}\mathbf{J}\tilde{\boldsymbol{i}}_{\mathrm{r}} - \boldsymbol{i}_{\mathrm{r0}}^{\mathrm{T}}\mathbf{J}\tilde{\boldsymbol{\psi}}_{\mathrm{r}} \tag{12}$$

The deviation of the magnetizing inductance can be written as

$$\begin{aligned}\tilde{L}_\mathrm{m} &= \left(\frac{\partial L_\mathrm{m}}{\partial i_\mathrm{m}}\frac{\partial i_\mathrm{m}}{\partial i_\mathrm{md}}\right)_0 \tilde{i}_\mathrm{md} + \left(\frac{\partial L_\mathrm{m}}{\partial i_\mathrm{m}}\frac{\partial i_\mathrm{m}}{\partial i_\mathrm{mq}}\right)_0 \tilde{i}_\mathrm{mq} \\ &\quad + \left(\frac{\partial L_\mathrm{m}}{\partial i_\mathrm{r}}\frac{\partial i_\mathrm{r}}{\partial i_\mathrm{rd}}\right)_0 \tilde{i}_\mathrm{rd} + \left(\frac{\partial L_\mathrm{m}}{\partial i_\mathrm{r}}\frac{\partial i_\mathrm{r}}{\partial i_\mathrm{rq}}\right)_0 \tilde{i}_\mathrm{rq} \\ &= \frac{L_\mathrm{mt0}-L_\mathrm{m0}}{i_\mathrm{m0}^2}\boldsymbol{i}_\mathrm{m0}^\mathrm{T}\tilde{\boldsymbol{i}}_\mathrm{m} + \frac{L_\mathrm{t0}}{i_\mathrm{m0}i_\mathrm{r0}}\boldsymbol{i}_\mathrm{r0}^\mathrm{T}\tilde{\boldsymbol{i}}_\mathrm{r}\end{aligned} \tag{13}$$

where $\tilde{\boldsymbol{i}}_\mathrm{m} = \tilde{\boldsymbol{i}}_\mathrm{s} + \tilde{\boldsymbol{i}}_\mathrm{r}$. Assuming no mutual saturation effect, i.e. $L_\mathrm{t0} = 0$, the deviation $\tilde{L}_\mathrm{m}$ of the magnetizing inductance is zero if the current deviation $\tilde{\boldsymbol{i}}_\mathrm{m}$ is perpendicular to the operating-point current $\boldsymbol{i}_\mathrm{m0}$. The deviation of the rotor leakage inductance $\tilde{L}_{\mathrm{r}\sigma}$ can be derived in a fashion similar to (13).

B. State-Space Representation

The deviations of the inductances $\tilde{L}_\mathrm{m}$ and $\tilde{L}_{\mathrm{r}\sigma}$ can be inserted into (11). Furthermore, $\tilde{\boldsymbol{i}}_\mathrm{s}$ and $\tilde{\boldsymbol{i}}_\mathrm{r}$ can be solved from (11) and inserted into (10), leading to a linear multiple-input state-space representation

$$\frac{\mathrm{d}\tilde{\boldsymbol{x}}}{\mathrm{d}t} = \boldsymbol{A}\tilde{\boldsymbol{x}} + \boldsymbol{B}_\mathrm{s}\tilde{\boldsymbol{u}}_\mathrm{s} + \boldsymbol{B}_\mathrm{r}\tilde{\boldsymbol{u}}_\mathrm{r} + \boldsymbol{b}\tilde{\omega}_\mathrm{m} \tag{14}$$

where the state vector and the input matrices are

$$\tilde{\boldsymbol{x}} = \begin{bmatrix}\tilde{\boldsymbol{\psi}}_\mathrm{s}\\ \tilde{\boldsymbol{\psi}}_\mathrm{r}\end{bmatrix},\quad \boldsymbol{B}_\mathrm{s} = \begin{bmatrix}\mathbf{I}\\ \mathbf{O}\end{bmatrix},\quad \boldsymbol{B}_\mathrm{r} = \begin{bmatrix}\mathbf{O}\\ \mathbf{I}\end{bmatrix},\quad \boldsymbol{b} = \begin{bmatrix}0\\ 0\\ \mathbf{J}\boldsymbol{\psi}_\mathrm{r0}\end{bmatrix} \tag{15}$$

The state matrix is

$$\boldsymbol{A} = -\begin{bmatrix}R_\mathrm{s}\mathbf{I} & \mathbf{O}\\ \mathbf{O} & R_\mathrm{r}\mathbf{I}\end{bmatrix}\boldsymbol{L}^{-1} - \begin{bmatrix}\omega_\mathrm{s0}\mathbf{J} & \mathbf{O}\\ \mathbf{O} & \omega_\mathrm{r0}\mathbf{J}\end{bmatrix} \tag{16}$$

where the inductance matrix is defined as

$$\begin{aligned}\boldsymbol{L} &= \begin{bmatrix}L_\mathrm{s0}\mathbf{I} & L_\mathrm{m0}\mathbf{I}\\ L_\mathrm{m0}\mathbf{I} & L_\mathrm{r0}\mathbf{I}\end{bmatrix} \\ &\quad + \frac{L_\mathrm{mt0}-L_\mathrm{m0}}{i_\mathrm{m0}^2}\begin{bmatrix}\boldsymbol{i}_\mathrm{m0}\boldsymbol{i}_\mathrm{m0}^\mathrm{T} & \boldsymbol{i}_\mathrm{m0}\boldsymbol{i}_\mathrm{m0}^\mathrm{T}\\ \boldsymbol{i}_\mathrm{m0}\boldsymbol{i}_\mathrm{m0}^\mathrm{T} & \boldsymbol{i}_\mathrm{m0}\boldsymbol{i}_\mathrm{m0}^\mathrm{T}\end{bmatrix} \\ &\quad + \frac{L_{\mathrm{r}\sigma\mathrm{t}0}-L_{\mathrm{r}\sigma0}}{i_\mathrm{r0}^2}\begin{bmatrix}\mathbf{O} & \mathbf{O}\\ \mathbf{O} & \boldsymbol{i}_\mathrm{r0}\boldsymbol{i}_\mathrm{r0}^\mathrm{T}\end{bmatrix} \\ &\quad + \frac{L_\mathrm{t0}}{i_\mathrm{m0}i_\mathrm{r0}}\begin{bmatrix}\mathbf{O} & \boldsymbol{i}_\mathrm{m0}\boldsymbol{i}_\mathrm{r0}^\mathrm{T}\\ \boldsymbol{i}_\mathrm{r0}\boldsymbol{i}_\mathrm{m0}^\mathrm{T} & \boldsymbol{i}_\mathrm{m0}\boldsymbol{i}_\mathrm{r0}^\mathrm{T} + \boldsymbol{i}_\mathrm{r0}\boldsymbol{i}_\mathrm{m0}^\mathrm{T}\end{bmatrix}\end{aligned} \tag{17}$$

The matrix $\boldsymbol{L}$ is symmetric due to the reciprocity conditions, and its last three terms originate from saturation.

The stator current, the rotor current, and the torque are chosen as output variables,

$$\tilde{\boldsymbol{i}}_\mathrm{s} = \boldsymbol{C}_\mathrm{s}\tilde{\boldsymbol{x}},\quad \tilde{\boldsymbol{i}}_\mathrm{r} = \boldsymbol{C}_\mathrm{r}\tilde{\boldsymbol{x}},\quad \tilde{T}_\mathrm{e} = \boldsymbol{c}\tilde{\boldsymbol{x}} \tag{18}$$

where the output matrices relating to the currents are

$$\boldsymbol{C}_\mathrm{s} = \begin{bmatrix}\mathbf{I} & \mathbf{O}\end{bmatrix}\boldsymbol{L}^{-1},\quad \boldsymbol{C}_\mathrm{r} = \begin{bmatrix}\mathbf{O} & \mathbf{I}\end{bmatrix}\boldsymbol{L}^{-1} \tag{19}$$

and the output matrix relating to the torque

$$\boldsymbol{c} = \boldsymbol{\psi}_\mathrm{r0}^\mathrm{T}\begin{bmatrix}\mathbf{O} & \mathbf{J}\end{bmatrix}\boldsymbol{L}^{-1} - \boldsymbol{i}_\mathrm{r0}^\mathrm{T}\begin{bmatrix}\mathbf{O} & \mathbf{J}\end{bmatrix} \tag{20}$$

in accordance with (12). The system can easily be analyzed using conventional tools for linear systems. If the saturation is not taken into account (i.e. $L_\mathrm{mt0} = L_\mathrm{m0}$, $L_{\mathrm{r}\sigma\mathrm{t}0} = L_{\mathrm{r}\sigma0}$, and $L_\mathrm{t0} = 0$), the small-signal model equals the conventional space-vector model. The model presented in [10] is obtained as a special case by choosing $L_{\mathrm{r}\sigma\mathrm{t}0} = L_{\mathrm{r}\sigma0}$ and $L_\mathrm{t0} = 0$.

C. Steady-State Relations

From (2) and (3), the steady-state condition

$$\begin{bmatrix}\boldsymbol{u}_\mathrm{s0}\\ \boldsymbol{u}_\mathrm{r0}\end{bmatrix} = \begin{bmatrix}R_\mathrm{s}\mathbf{I} + \omega_\mathrm{s0}L_\mathrm{s0}\mathbf{J} & \omega_\mathrm{s0}L_\mathrm{m0}\mathbf{J}\\ \omega_\mathrm{r0}L_\mathrm{m0}\mathbf{J} & R_\mathrm{r}\mathbf{I} + \omega_\mathrm{r0}L_\mathrm{r0}\mathbf{J}\end{bmatrix}\begin{bmatrix}\boldsymbol{i}_\mathrm{s0}\\ \boldsymbol{i}_\mathrm{r0}\end{bmatrix} \tag{21}$$

is obtained. The operating-point voltages can thus be determined if the parameters and the operating-point currents are known.

In many applications, the stator voltage $\boldsymbol{u}_\mathrm{s0}$, the stator current $\boldsymbol{i}_\mathrm{s0}$, and the stator angular frequency ω_s0 are known in the operating point. Furthermore, the rotor winding is typically short-circuited, and the rotor current $\boldsymbol{i}_\mathrm{r0}$ is inaccessible. Therefore, it is useful to solve the rotor current from (21),

$$\boldsymbol{i}_\mathrm{r0} = -\mathbf{J}\left[\boldsymbol{u}_\mathrm{s0} - (R_\mathrm{s}\mathbf{I} + \omega_\mathrm{s0}L_\mathrm{s0}\mathbf{J})\boldsymbol{i}_\mathrm{s0}\right]/(\omega_\mathrm{s0}L_\mathrm{m0}) \tag{22}$$

Hence, the magnetizing current $\boldsymbol{i}_\mathrm{m0} = \boldsymbol{i}_\mathrm{s0} + \boldsymbol{i}_\mathrm{r0}$ and the rotor flux $\boldsymbol{\psi}_\mathrm{r0} = L_\mathrm{m0}\boldsymbol{i}_\mathrm{s0} + L_\mathrm{r0}\boldsymbol{i}_\mathrm{r0}$ needed in the linearized model can be calculated.

In addition to $\boldsymbol{i}_\mathrm{r0}$, two parameters can be solved from (21). Convenient choices are the rotor resistance and the rotor inductance:

$$R_\mathrm{r} = \boldsymbol{i}_\mathrm{r0}^\mathrm{T}(\boldsymbol{u}_\mathrm{r0} - \omega_\mathrm{r0}L_\mathrm{m0}\mathbf{J}\boldsymbol{i}_\mathrm{s0})/i_\mathrm{r0}^2 \tag{23}$$

$$L_\mathrm{r0} = -\boldsymbol{i}_\mathrm{r0}^\mathrm{T}\mathbf{J}(\boldsymbol{u}_\mathrm{r0} - \omega_\mathrm{r0}L_\mathrm{m0}\mathbf{J}\boldsymbol{i}_\mathrm{s0})/(\omega_\mathrm{r0}i_\mathrm{r0}^2) \tag{24}$$

The rotor leakage inductance needed in the model is $L_{\mathrm{r}\sigma0} = L_\mathrm{r0} - L_\mathrm{m0}$. If the linearized model is used for parameter estimation or fitting, the information in (21) should be used to avoid inconsistency with the operating-point data. Furthermore, the fitting procedure becomes easier, since the number of independent parameters decreases. If the operating-point stator voltage $\boldsymbol{u}_\mathrm{s0}$ is unknown, it may be useful to express the rotor current as

$$\boldsymbol{i}_\mathrm{r0} = \left(\alpha_0\mathbf{I} + \omega_\mathrm{r0}\mathbf{J}\right)^{-1}\left(\boldsymbol{u}_\mathrm{r0} - \omega_\mathrm{r0}L_\mathrm{m0}\mathbf{J}\boldsymbol{i}_\mathrm{s0}\right)/L_\mathrm{r0} \tag{25}$$

where $\alpha_0 = R_\mathrm{r}/L_\mathrm{r0}$ is the inverse rotor time constant.

IV. Transfer Functions

The stator current can be expressed as $\tilde{\boldsymbol{i}}_\mathrm{s}(s) = \boldsymbol{Y}_\mathrm{s}(s)\tilde{\boldsymbol{u}}_\mathrm{s}(s)$, where the multiple-input-multiple-output transfer function matrix (or the small-signal stator-admittance matrix) is

$$\boldsymbol{Y}_\mathrm{s}(s) = \begin{bmatrix}Y_\mathrm{dd}(s) & Y_\mathrm{dq}(s)\\ Y_\mathrm{qd}(s) & Y_\mathrm{qq}(s)\end{bmatrix} = \boldsymbol{C}_\mathrm{s}\left(s\mathbf{I}_4 - \boldsymbol{A}\right)^{-1}\boldsymbol{B}_\mathrm{s} \tag{26}$$

where $\mathbf{I}_4$ is a 4×4 identity matrix. The expression (26) is valid in any synchronous coordinates. An admittance matrix $\boldsymbol{Y}_\mathrm{s}(s)$ can be represented in new synchronous coordinates as

$$\boldsymbol{Y}_\mathrm{s}'(s) = \mathrm{e}^{\vartheta_0\mathbf{J}}\boldsymbol{Y}_\mathrm{s}(s)\mathrm{e}^{-\vartheta_0\mathbf{J}} \tag{27}$$

where ϑ_0 is the angle of the d axis of original coordinates in new coordinates. The coordinate transformation matrix can be expressed as $\mathrm{e}^{\vartheta_0\mathbf{J}} = \cos(\vartheta_0)\mathbf{I} + \sin(\vartheta_0)\mathbf{J}$. In the case of no saturation, $\boldsymbol{Y}_\mathrm{s}(s) = Y_\mathrm{dd}(s)\mathbf{I} + Y_\mathrm{qd}(s)\mathbf{J} = \boldsymbol{Y}_\mathrm{s}'(s)$ holds, and the admittance matrix does not depend on the angle ϑ_0.

In the unsaturated case, the system could be expressed as a complex-valued single-input-single-output transfer function for complex-valued space vectors.

When the stator current is considered as the input of the system, the reciprocal relationship $\tilde{\boldsymbol{u}}_\mathrm{s}(s) = \boldsymbol{Z}_\mathrm{s}(s)\tilde{\boldsymbol{i}}_\mathrm{s}(s)$ can be used, where the small-signal stator-impedance matrix is $\boldsymbol{Z}_\mathrm{s}(s) = \boldsymbol{Y}_\mathrm{s}^{-1}(s)$. If the saturation is not taken into account, the stator-impedance matrix reduces to the well-known expression

$$\begin{aligned}\boldsymbol{Z}_\mathrm{s}(s) = {} & R_{\sigma 0}\mathbf{I} + (s\mathbf{I} + \omega_{\mathrm{s}0}\mathbf{J})L_{\sigma 0} \\ & - k_{\mathrm{r}0}^2 R_\mathrm{r}(\alpha_0\mathbf{I} - \omega_{\mathrm{m}0}\mathbf{J})\left(s\mathbf{I} + \alpha_0\mathbf{I} + \omega_{\mathrm{r}0}\mathbf{J}\right)^{-1}\end{aligned} \tag{28}$$

where the total leakage inductance and the total resistance are

$$L_{\sigma 0} = L_{\mathrm{s}\sigma} + k_{\mathrm{r}0}L_{\mathrm{r}\sigma 0}, \quad R_{\sigma 0} = R_\mathrm{s} + k_{\mathrm{r}0}^2 R_\mathrm{r} \tag{29}$$

respectively, and $k_{\mathrm{r}0} = L_{\mathrm{m}0}/L_{\mathrm{r}0}$ is the magnetic coupling factor of the rotor.

If torsional dynamics are of interest [15], [16], the transfer function from the rotor speed to the electromagnetic torque is needed. The electromagnetic torque can be expressed as $\tilde{T}_\mathrm{e}(s) = G(s)\tilde{\omega}_\mathrm{m}(s)$, where the single-input-single-output transfer function is

$$G(s) = \boldsymbol{c}\left(s\mathbf{I}_4 - \boldsymbol{A}\right)^{-1}\boldsymbol{b} \tag{30}$$

In a fashion similar to (26) and (30), other transfer-function matrices can be obtained using (14) and (18).

V. Reduced-Order Stator Impedance

A short-circuited rotor winding is considered here, i.e. $\boldsymbol{u}_\mathrm{r} = [0, 0]^\mathrm{T}$. At higher frequencies, the stator-impedance matrix can be approximated as

$$\boldsymbol{Z}_\mathrm{s}(s) = \boldsymbol{R}_\sigma + (s\mathbf{I} + \omega_{\mathrm{s}0}\mathbf{J})\,\boldsymbol{L}_\sigma \tag{31}$$

where $\boldsymbol{L}_\sigma$ is the total leakage inductance matrix and $\boldsymbol{R}_\sigma$ is the total resistance matrix. The derivation of (31) and the expressions for $\boldsymbol{L}_\sigma$ and $\boldsymbol{R}_\sigma$ are given in Appendix B.

The effects of the rotor leakage inductance saturation are more prominent at high frequencies while the saturation of the magnetizing inductance mainly affects at low frequencies. Omitting the saturation of the magnetizing inductance and the effect of the main flux on the rotor leakage inductance as well, i.e. $L_{\mathrm{m}t0} = L_{\mathrm{m}0}$ and $L_{\mathrm{t}0} = 0$, yields

$$\begin{aligned}\boldsymbol{L}_\sigma &= L_{\sigma 0}\mathbf{I} + (L_{\sigma \mathrm{t}0} - L_{\sigma 0})\frac{\boldsymbol{i}_{\mathrm{r}0}\boldsymbol{i}_{\mathrm{r}0}^\mathrm{T}}{i_{\mathrm{r}0}^2} \\ &= \mathrm{e}^{\vartheta_{\mathrm{r}0}\mathbf{J}}\begin{bmatrix} L_{\sigma \mathrm{t}0} & 0 \\ 0 & L_{\sigma 0}\end{bmatrix}\mathrm{e}^{-\vartheta_{\mathrm{r}0}\mathbf{J}}\end{aligned} \tag{32}$$

$$\begin{aligned}\boldsymbol{R}_\sigma &= R_{\sigma 0}\mathbf{I} + (R_{\sigma \mathrm{t}0} - R_{\sigma 0})\frac{\boldsymbol{i}_{\mathrm{r}0}\boldsymbol{i}_{\mathrm{r}0}^\mathrm{T}}{i_{\mathrm{r}0}^2} \\ &= \mathrm{e}^{\vartheta_{\mathrm{r}0}\mathbf{J}}\begin{bmatrix} R_{\sigma \mathrm{t}0} & 0 \\ 0 & R_{\sigma 0}\end{bmatrix}\mathrm{e}^{-\vartheta_{\mathrm{r}0}\mathbf{J}}\end{aligned} \tag{33}$$

where $\vartheta_{\mathrm{r}0}$ is the angle of the operating-point rotor current vector. The incremental total leakage inductance and the incremental total resistance are

$$L_{\sigma \mathrm{t}0} = L_{\mathrm{s}\sigma} + k_{\mathrm{rt}0}L_{\mathrm{r}\sigma \mathrm{t}0}, \quad R_{\sigma \mathrm{t}0} = R_\mathrm{s} + k_{\mathrm{rt}0}^2 R_\mathrm{r} \tag{34}$$

respectively, where $k_{\mathrm{rt}0} = L_{\mathrm{m}0}/(L_{\mathrm{m}0} + L_{\mathrm{r}\sigma \mathrm{t}0})$. It is worth noticing that both the total leakage inductance matrix and the total resistance matrix depend on the angle $\vartheta_{\mathrm{r}0}$ if the machine is saturated. Under the assumptions $L_{\mathrm{m}t0} = L_{\mathrm{m}0}$ and $L_{\mathrm{t}0} = 0$, the impedance (31) can be written as

$$\boldsymbol{Z}_\mathrm{s}(s) = \mathrm{e}^{\vartheta_{\mathrm{r}0}\mathbf{J}}\begin{bmatrix} R_{\sigma \mathrm{t}0} + sL_{\sigma \mathrm{t}0} & -\omega_{\mathrm{s}0}L_{\sigma 0} \\ \omega_{\mathrm{s}0}L_{\sigma \mathrm{t}0} & R_{\sigma 0} + sL_{\sigma 0}\end{bmatrix}\mathrm{e}^{-\vartheta_{\mathrm{r}0}\mathbf{J}} \tag{35}$$

According to the approximate reduced-order model (35), the saturation of the rotor leakage inductance provides information of the direction of the operating-point rotor current vector $\boldsymbol{i}_{\mathrm{r}0}$ (or the vector $-\mathbf{J}\boldsymbol{\psi}_{\mathrm{r}0}$ since $\boldsymbol{u}_{\mathrm{r}0} = [0, 0]^\mathrm{T}$ is assumed). These saturation-induced saliencies related to the direction of $\boldsymbol{\psi}_{\mathrm{r}0}$ may be exploited in flux-angle estimation, e.g. [5], [6]. Furthermore, these saliencies should be taken into account when adapting $L_{\sigma 0}$ and $R_{\sigma 0}$ using signal-injection methods similar to [17]. However, since the assumption $L_{\mathrm{t}0} = 0$ does not usually hold for machines with skewed or closed rotor slots, the approximate reduced-order model (35) should be used with care.

VI. Results

Small-signal characteristics of a 2.2-kW squirrel-cage induction machine were studied by means of two-dimensional time-stepping FEA [13] and laboratory experiments. The machine is equipped with closed and skewed rotor slots, and its rating is: voltage 400 V; current 5 A; frequency 50 Hz; speed 1436 r/min; and torque 14.6 Nm. The base values are: angular frequency $2\pi 50$ rad/s; voltage $\sqrt{2/3}\cdot 400$ V; and current $\sqrt{2}\cdot 5$ A.

A. Finite-Element Analysis at Rated Operating Point

Three different kinds of tests were carried out using time-stepping FEA: the voltage-pulse test; the pulsating voltage-signal injection test; and the speed-pulse test. Parameters of the proposed model were identified based on the data from the voltage-pulse test, and the predictions of the model are compared with the results from the other two independent tests. The rated operating point is considered. The skewing of the rotor slots is not modeled in FEA.

1) Voltage-Pulse Test: Several frequencies can be simultaneously excited by means of a pulse test. Hence, the number of time-stepping FEA simulations required for gathering frequency-response data can be significantly reduced as compared to harmonic excitation. Here, the voltage pulse is defined by [14]

$$\tilde{u}_\mathrm{s} = \begin{cases} u_\delta \sin^2(\omega_\delta t), & 0 \le t \le 1/(2\omega_\delta) \\ 0, & \text{otherwise}\end{cases} \tag{36}$$

where $u_\delta = 0.1$ p.u. and ω_δ = 4 p.u. The duration time $1/(2\omega_\delta)$ corresponds to 2.5 ms. The pulse test was performed twice with perpendicular pulses, whose directions are illustrated in Figs. 3(a) and 3(b). The pulse was first applied to the d direction, i.e. $\tilde{\boldsymbol{u}}_\mathrm{s} = [\tilde{u}_\mathrm{s}, 0]^\mathrm{T}$, and then to the q direction, i.e. $\tilde{\boldsymbol{u}}_\mathrm{s} = [0, \tilde{u}_\mathrm{s}]^\mathrm{T}$; the d axis is aligned with the operating-point stator voltage.

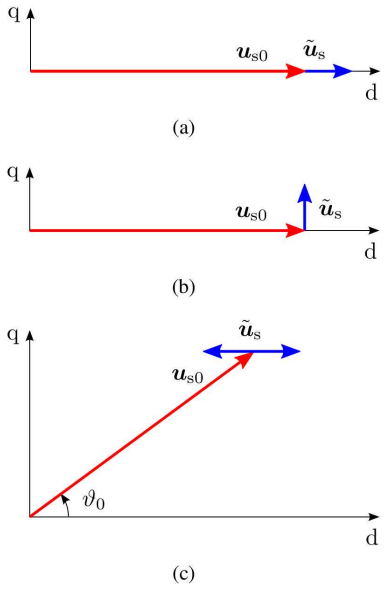

Fig. 3. Excitation voltages: (a) pulse applied to $\tilde{u}_{sd}$ in operating-point stator-voltage coordinates; (b) pulse applied to $\tilde{u}_{sq}$ in operating-point stator-voltage coordinates; (c) pulsating voltage $\tilde{u}_{sd} = u_c \sin(\omega t)$ in arbitrary coordinates.

The results of time-stepping computations were transformed to the frequency domain using DFT. Since two pulse tests were made, it was possible to calculate all four small-signal admittances $Y_{dd}(j\omega)$, $Y_{dq}(j\omega)$, $Y_{qd}(j\omega)$, and $Y_{qq}(j\omega)$. The circles and crosses in Fig. 4 show the admittances from the FEA data in the operating-point stator voltage coordinates. If the motor were not saturated, the circles and crosses would overlap.

The admittance matrix (26) of the proposed model was fitted to the frequency response data obtained from time-stepping FEA. The inductances $L_{s\sigma}$, L_{m0}, L_{mt0}, $L_{r\sigma t0}$, and L_{t0} and the stator resistance R_s were allowed to vary freely in the data fitting. These parameters together with the operating-point data ($\boldsymbol{u}_{s0}$, $\boldsymbol{i}_{s0}$, ω_{s0}, and ω_{r0}) obtained from FEA were used to calculate the operating-point rotor current from (22), R_r from (23), and $L_{r\sigma 0} = L_{r0} - L_{m0}$ from (24). An estimate of the admittance matrix was calculated according to (26). The cost function used in the data fitting is the sum of the square errors of the elements in the admittance matrix. The result of the data fitting is presented in Fig. 4 by solid lines. As can be seen, the model fits rather well to the data. At frequencies close to 3 p.u., the influence of the skin effect begins to decrease the goodness of the fit. If needed, the skin effect could be taken into account by an additional rotor branch [18]. Table I gives the parameters obtained by fitting the proposed model using the FEA data shown in Fig. 4. The fitted parameters are physically reasonable, and they are consistent with the operating point.

For comparison, the model (26) with the assumptions $L_{r\sigma t0} = L_{r\sigma 0}$ and $L_{t0} = 0$, corresponding to the model in [10], was investigated. The model fits well if only the lowest frequencies (below 0.2 p.u.) are used. At higher frequencies, the saturation of the rotor leakage inductance and the mutual saturation effect decrease the goodness of the fit significantly

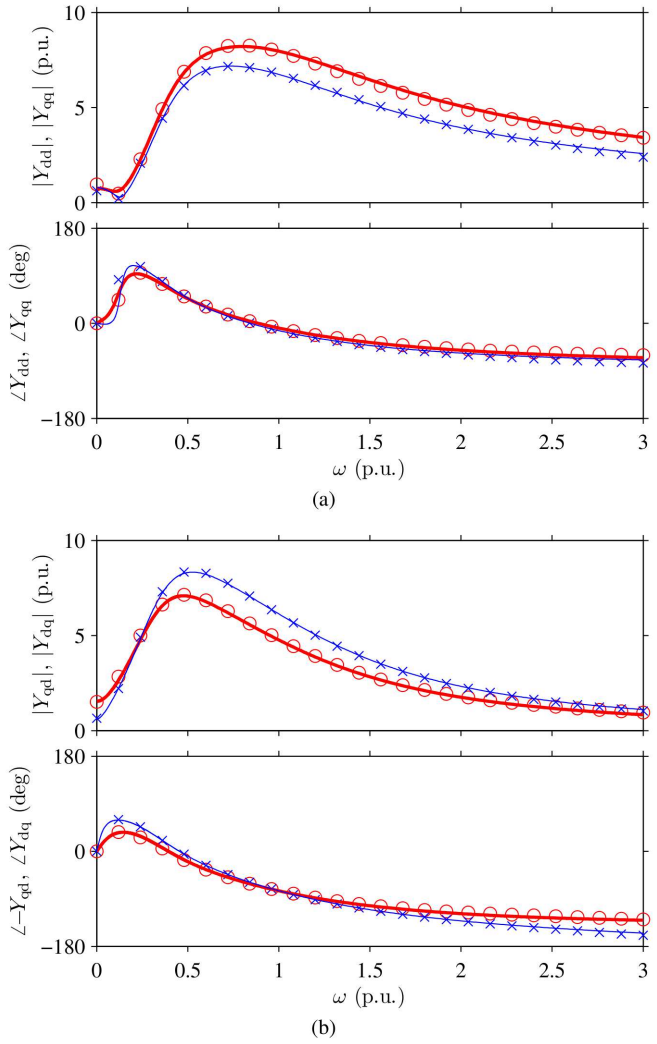

Fig. 4. Admittances from time-stepping FEA (circles and crosses) and from fitted model (26) (solid lines) in coordinates fixed to $\boldsymbol{u}_{s0}$: (a) $Y_{dd}(j\omega)$ shown by thick line and circles, $Y_{qq}(j\omega)$ shown by thin line and crosses; (b) $Y_{qd}(j\omega)$ shown by thick line and circles, $Y_{dq}(j\omega)$ shown by thin line and crosses. In the case of no saturation, conditions $Y_{dd}(j\omega) = Y_{qq}(j\omega)$ and $Y_{qd}(j\omega) = -Y_{dq}(j\omega)$ would hold.

(or nonphysical parameter values are obtained as a result).

In some applications, the stator impedance matrix may be preferred over the stator admittance matrix. Solid lines in Fig. 5 show the stator impedances corresponding to the fitted admittances in Fig. 4. The d axis is aligned with the operating-point stator voltage. The dashed lines present the impedances calculated using the reduced-order model (31). The curves differ significantly at low frequencies but they practically overlap at frequencies above 1 p.u.

2) Pulsating Voltage-Signal Injection Test: The pulsating excitation voltage was applied in time-stepping FEA in the direction of the d axis of a synchronously rotating coordinate system, i.e. $\tilde{\boldsymbol{u}}_s = [u_c \sin(\omega t), 0]^T$. The amplitude $u_c = 0.025$ p.u. and the angular frequency $\omega = 1.2$ p.u. were used. The resulting small-signal current responses $\tilde{i}_{sd}$ and $\tilde{i}_{sq}$ were transformed to the frequency domain, and the small-signal stator admittances $Y_{dd}(j\omega)$ and $Y_{qd}(j\omega)$ were calculated. To

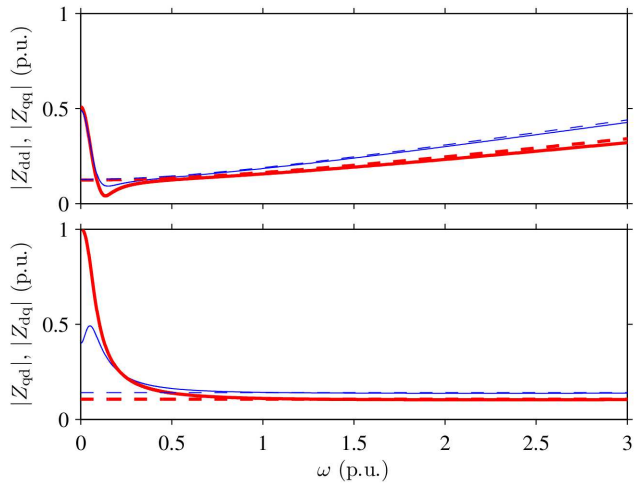

Fig. 5. Impedances corresponding to Fig. 4 shown by solid lines and impedances from the reduced-order model (31) shown by dashed lines. The d axis is aligned with $\boldsymbol{u}_{\mathrm{s}0}$. In the case of no saturation, conditions $Z_{\mathrm{dd}}(\mathrm{j}\omega) = Z_{\mathrm{qq}}(\mathrm{j}\omega)$ and $Z_{\mathrm{dq}}(\mathrm{j}\omega) = -Z_{\mathrm{qd}}(\mathrm{j}\omega)$ would hold.

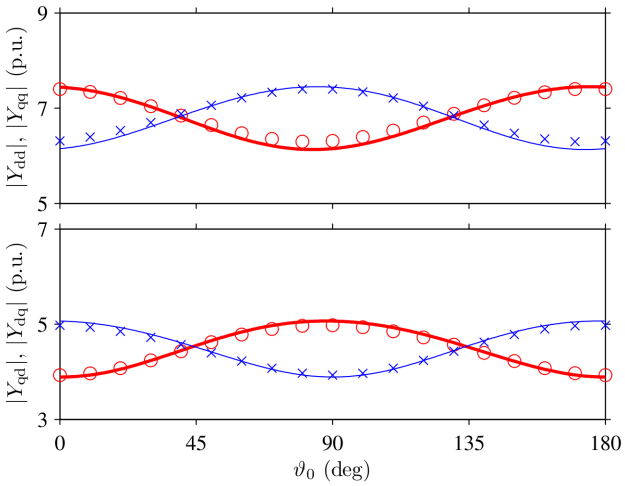

Fig. 6. Admittances at excitation frequency $\omega = 1.2$ p.u. as a function of the angle ϑ_0 of vector $\boldsymbol{u}_{\mathrm{s}0}$. Circles and crosses are the admittances calculated based on the signal-injection tests carried out in time-stepping FEA. The solid lines are obtained using (26) and the fitted parameters corresponding to Fig. 4. In the case of no saturation, the admittances would be independent of ϑ_0.

TABLE I
PER-UNIT PARAMETERS AND OPERATING POINT IN FIG. 4

Parameter	Value	Source
R_{s}	0.080	Fitted
R_{r}	0.047	Eq. (23)
$L_{\mathrm{s}\sigma}$	0.087	Fitted
$L_{\mathrm{m}0}$	1.584	Fitted
$L_{\mathrm{r}\sigma 0}$	0.055	Eq. (24)
$L_{\mathrm{mt}0}$	0.506	Fitted
$L_{\mathrm{r}\sigma \mathrm{t}0}$	0.019	Fitted
$L_{\mathrm{t}0}$	−0.069	Fitted
$\omega_{\mathrm{s}0}$	1.000	FEA
$\omega_{\mathrm{r}0}$	0.043	FEA
$\boldsymbol{u}_{\mathrm{s}0}$	$1.00\angle 0°$	FEA
$\boldsymbol{i}_{\mathrm{s}0}$	$0.99\angle -38°$	FEA
$\boldsymbol{i}_{\mathrm{r}0}$	$0.80\angle 176°$	Eq. (22)

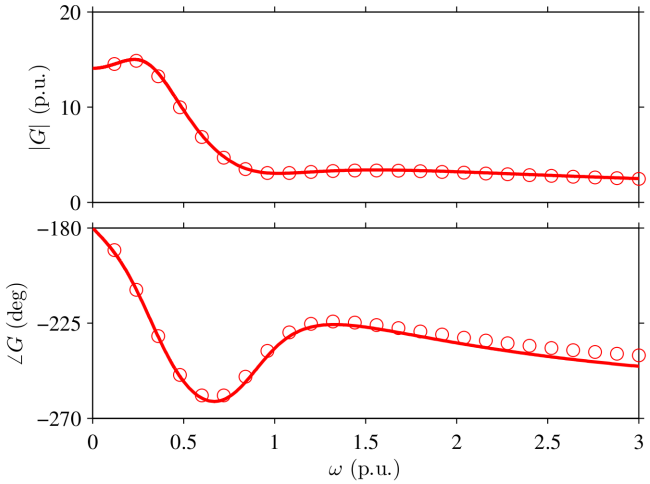

Fig. 7. Frequency response $G(\mathrm{j}\omega) = \tilde{T}_{\mathrm{e}}(\mathrm{j}\omega)/\tilde{\omega}_{\mathrm{m}}(\mathrm{j}\omega)$. The solid lines are obtained using (30) and the fitted parameters corresponding to Fig. 4. Circles are calculated based on the speed-pulse test carried out in time-stepping FEA.

evaluate the effect of the direction of the excitation signal on the admittances, the direction of the excitation signal (i.e. the orientation of the d axis) was varied with respect to the operating-point stator voltage as illustrated in Fig. 3(c); the angle ϑ_0 was varied in steps of 10°. The d axis is aligned with the operating-point stator voltage at $\vartheta_0 = 0$.

The admittances obtained using the pulsating voltage-signal injection tests are depicted in Fig. 6. It can be seen that the admittances depend significantly on the angle ϑ_0. For comparison, the admittances corresponding to the proposed model are shown by the solid lines in the figure. These admittances were calculated using (26) with the parameters in Table I and the coordinate transformation (27). It can be seen that the proposed model fits very well to the data from the signal-injection test. It is worth noticing that $Y_{\mathrm{qq}}(\vartheta_0) = Y_{\mathrm{dd}}(\vartheta_0 - \pi/2)$ and $Y_{\mathrm{dq}}(\vartheta_0) = -Y_{\mathrm{qd}}(\vartheta_0 - \pi/2)$.

3) Speed-Pulse Test: The transfer function from the rotor speed to the electromagnetic torque was investigated by applying an pulse to the speed while the motor was supplied by a sinusoidal voltage in time-stepping FEA [19]. Transforming this data into the frequency domain, the frequency response shown by the circles in Fig. 7 is obtained. For comparison, the frequency response was calculated using (30) and the parameter values given in Table I. This transfer function is shown in Fig. 7 by the solid line. It can be observed that the proposed model fits well to the data from the speed pulse test. Hence, the fitted parameter values—obtained from the voltage-pulse tests—are consistent with the data from the speed-pulse test.

B. Experiments Under Locked-Rotor Condition

In the laboratory experiments, a 2.2-kW induction machine was fed by a frequency converter controlled by a dSPACE DS1103 PPC/DSP board. The rotor was mechanically locked; this operating condition was chosen to ensure that there is no oscillation in the rotor speed, i.e. $\tilde{\omega}_{\mathrm{m}} = 0$ holds. The stator

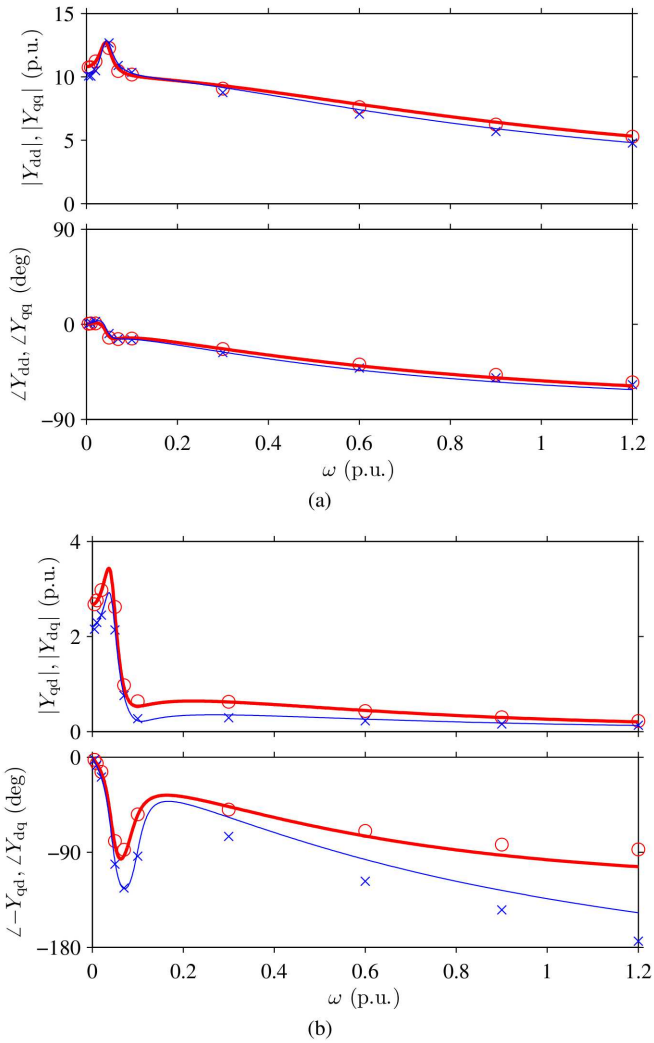

Fig. 8. Admittances from measurements (circles and crosses) and from fitted model (26) (solid lines) in coordinates fixed to $\boldsymbol{u}_{s0}$: (a) $Y_{dd}(j\omega)$ shown by thick line and circles, $Y_{qq}(j\omega)$ shown by thin line and crosses; (b) $Y_{qd}(j\omega)$ shown by thick line and circles, $Y_{dq}(j\omega)$ shown by thin line and crosses. In the case of no saturation, conditions $Y_{dd}(j\omega) = Y_{qq}(j\omega)$ and $Y_{qd}(j\omega) = -Y_{dq}(j\omega)$ would hold.

frequency was equal to the rated slip frequency. The magnitude of the operating-point voltage was adjusted so that the rated stator current is obtained.

To reduce the influence of the measurement noise, the voltage-pulse test was not used in the laboratory experiments. Instead, the small-signal admittance was measured at several frequencies, one at a time, using the pulsating voltage-signal injection tests. To evaluate all four elements in the admittance matrix, the voltage signals were injected in two perpendicular directions: first at $\vartheta_0 = 0°$ and then at $\vartheta_0 = 90°$ in accordance with Fig. 3(c). The circles and crosses in Fig. 8 show the measured admittances in the operating-point stator voltage coordinates.

The admittance matrix (26) of the proposed model was fitted to the measured frequency response data as described in Section VI-A1. The result of the data fitting is presented in Fig. 8 by the solid lines, and the corresponding parameters are

TABLE II
PER-UNIT PARAMETERS AND OPERATING POINT IN FIG. 8

Parameter	Value for proposed model	Value for model in [10]	Source
R_s	0.065	0.065	Fitted
R_r	0.040	0.040	Eq. (23)
$L_{s\sigma}$	0.025	0.022	Fitted
L_{m0}	1.853	1.752	Fitted
$L_{r\sigma 0}$	0.140	0.130	Eq. (24)
L_{mt0}	1.245	1.274	Fitted
$L_{r\sigma t0}$	0.121	–	Fitted
L_{t0}	−0.059	–	Fitted
ω_{s0}	0.043	0.043	Measured
ω_{r0}	0.043	0.043	Measured
$\boldsymbol{u}_{s0}$	$0.09\angle 0°$	$0.09\angle 0°$	Measured
$\boldsymbol{i}_{s0}$	$1.00\angle -12°$	$1.00\angle -12°$	Measured
$\boldsymbol{i}_{r0}$	$0.84\angle -167°$	$0.83\angle -166°$	Eq. (22)

given in Table II. It can be seen that the proposed model fits well and the fitted parameters are physically reasonable. The small differences between the measured and fitted admittances may originate from measurement errors and from phenomena omitted in the model (e.g., skin effect and iron losses).

The effect of the direction of the excitation signal on the small-signal admittance was also analyzed. The voltage signal pulsating at the frequency $\omega = 1.2$ p.u. was used; the angle ϑ_0 was varied in steps of 10° with respect to the operating-point stator voltage, cf. Fig. 3(c). The measured admittances are shown by the circles in Fig. 9. The admittances corresponding to the proposed model are shown by the thick lines in the figure. These admittances were calculated using (26) with the parameters in Table II and the coordinate transformation (27). It can be seen that the proposed model can predict the admittance as a function of the direction of the excitation signal. It is to be noted that the temperature and the resistances increased while performing the test at different angles. In Fig. 9, the measured admittances at $\vartheta_0 = 180°$ differ from those at $\vartheta_0 = 0°$ mainly due to the temperature rise.

For comparison, the model (26) with the assumptions $L_{r\sigma t0} = L_{r\sigma 0}$ and $L_{t0} = 0$, corresponding to the model in [10], was fitted to the measured data shown in Fig. 8. The fitted parameters are given in Table II. The model fits well only at the lowest excitation frequencies. As an example, the admittance at the excitation frequency $\omega = 1.2$ p.u. as a function of the excitation-signal angle ϑ_0 is depicted by the thin lines in Fig. 9. It can be observed that the prediction from the proposed model is superior to that from the model in [10].

VII. CONCLUSIONS

The magnetic saturation can be taken into account when deriving a small-signal model for the induction machine. The proposed model takes into account the mutual saturation effect originating mainly from skewed and closed rotor slots, and it fulfills the reciprocity conditions. The model can be applied to parameter identification and to the analysis and development of flux angle estimation methods. Furthermore, the small-signal relationship between the rotor speed and the electromagnetic torque—needed if torsional dynamics are

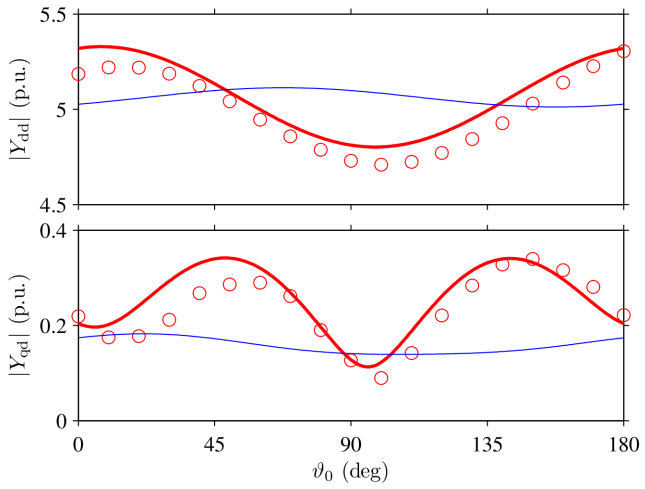

Fig. 9. Measured admittances (circles) as a function of excitation-signal angle ϑ_0 at frequency ω = 1.2 p.u. The rotor is locked, the stator frequency equals the rated slip frequency, and the stator current equals its rated value. Thick lines are calculated using the proposed model (26), and the thin lines are calculated using the model in [10]. Parameters given in Table II are used.

analyzed—can be evaluated. At higher frequencies, a reduced-order small-signal model can be used; magnetic saturation makes both the total leakage inductance and the total resistance salient. As application examples, the machine parameters were identified using the data obtained from time-stepping finite-element analysis and locked-rotor measurements. Based on the results, the mutual saturation can have significant effect on the small-signal characteristics of the induction machine.

Appendix A
Reciprocity Conditions

The reciprocity conditions given in (7) are related to the T model shown in Fig. 1. More generally, the magnetic coupling between $\boldsymbol{i}_{\mathrm{s}}$, $\boldsymbol{\psi}_{\mathrm{s}}$ and $\boldsymbol{i}_{\mathrm{r}}$, $\boldsymbol{\psi}_{\mathrm{r}}$ can be modeled as a multi-terminal (or multi-port) inductor. If a flux-controlled or current-controlled inductor is lossless, it is reciprocal [11]. The incremental inductance matrix associated with a reciprocal multi-terminal inductor is symmetric, leading to the reciprocity conditions

$$\frac{\partial\psi_{\mathrm{sd}}}{\partial i_{\mathrm{sq}}}=\frac{\partial\psi_{\mathrm{sq}}}{\partial i_{\mathrm{sd}}},\quad \frac{\partial\psi_{\mathrm{sd}}}{\partial i_{\mathrm{rd}}}=\frac{\partial\psi_{\mathrm{rd}}}{\partial i_{\mathrm{sd}}},\quad \frac{\partial\psi_{\mathrm{sd}}}{\partial i_{\mathrm{rq}}}=\frac{\partial\psi_{\mathrm{rq}}}{\partial i_{\mathrm{sd}}} \qquad (37)$$
$$\frac{\partial\psi_{\mathrm{sq}}}{\partial i_{\mathrm{rd}}}=\frac{\partial\psi_{\mathrm{rd}}}{\partial i_{\mathrm{sq}}},\quad \frac{\partial\psi_{\mathrm{sq}}}{\partial i_{\mathrm{rq}}}=\frac{\partial\psi_{\mathrm{rq}}}{\partial i_{\mathrm{sq}}},\quad \frac{\partial\psi_{\mathrm{rd}}}{\partial i_{\mathrm{rq}}}=\frac{\partial\psi_{\mathrm{rq}}}{\partial i_{\mathrm{rd}}}$$

These conditions can also be obtained from (6) assuming the magnetic field to be conservative.

Appendix B
Derivation of Reduced-Order Model

To derive a reduced-order stator-impedance matrix for higher frequencies, a new state vector $\tilde{\boldsymbol{z}}$ is defined,

$$\tilde{\boldsymbol{z}}=\begin{bmatrix}\tilde{\boldsymbol{i}}_{\mathrm{s}}\\ \tilde{\boldsymbol{\psi}}_{\mathrm{r}}\end{bmatrix}=\begin{bmatrix}\boldsymbol{C}_{\mathrm{s}} & \\ \mathbf{O} & \mathbf{I}\end{bmatrix}\tilde{\boldsymbol{x}}=\boldsymbol{T}^{-1}\tilde{\boldsymbol{x}} \qquad (38)$$

yielding the state-space representation

$$\frac{\mathrm{d}\tilde{\boldsymbol{z}}}{\mathrm{d}t}=\boldsymbol{F}\tilde{\boldsymbol{z}}+\boldsymbol{G}_{\mathrm{s}}\tilde{\boldsymbol{u}}_{\mathrm{s}}+\boldsymbol{G}_{\mathrm{r}}\tilde{\boldsymbol{u}}_{\mathrm{r}}+\boldsymbol{g}\tilde{\omega}_{\mathrm{m}} \qquad (39)$$

where the system matrices are $\boldsymbol{G}_{\mathrm{r}}=\boldsymbol{T}^{-1}\boldsymbol{B}_{\mathrm{r}}$, $\boldsymbol{g}=\boldsymbol{T}^{-1}\boldsymbol{b}$, and

$$\boldsymbol{F}=\boldsymbol{T}^{-1}\boldsymbol{A}\boldsymbol{T}=\begin{bmatrix}\boldsymbol{F}_{11} & \boldsymbol{F}_{12}\\ \boldsymbol{F}_{21} & \boldsymbol{F}_{22}\end{bmatrix} \qquad (40)$$

$$\boldsymbol{G}_{\mathrm{s}}=\boldsymbol{T}^{-1}\boldsymbol{B}_{\mathrm{s}}=\begin{bmatrix}\boldsymbol{G}_{\mathrm{s1}}\\ \boldsymbol{G}_{\mathrm{s2}}\end{bmatrix} \qquad (41)$$

Since $\tilde{\omega}_{\mathrm{m}}$ does not affect the stator impedance, $\tilde{\omega}_{\mathrm{m}}=0$ will be assumed for simplicity in the following. Furthermore, a short-circuited rotor winding is considered, i.e. $\boldsymbol{u}_{\mathrm{r}}=[0,0]^{\mathrm{T}}$. The stator-current dynamics are usually significantly faster than the rotor-flux dynamics. Hence, $\tilde{\boldsymbol{\psi}}_{\mathrm{r}}=[0,0]^{\mathrm{T}}$ can be assumed at higher frequencies, and the state-space representation (39) reduces to

$$\boldsymbol{L}_{\sigma}\frac{\mathrm{d}\tilde{\boldsymbol{i}}_{\mathrm{s}}}{\mathrm{d}t}=\tilde{\boldsymbol{u}}_{\mathrm{s}}-\boldsymbol{R}_{\sigma}\tilde{\boldsymbol{i}}_{\mathrm{s}}-\omega_{\mathrm{s0}}\mathbf{J}\boldsymbol{L}_{\sigma}\tilde{\boldsymbol{i}}_{\mathrm{s}} \qquad (42)$$

where the total leakage inductance matrix is $\boldsymbol{L}_{\sigma}=\boldsymbol{G}_{\mathrm{s1}}^{-1}$ and the total resistance matrix is $\boldsymbol{R}_{\sigma}=-\boldsymbol{L}_{\sigma}\boldsymbol{F}_{11}-\omega_{\mathrm{s0}}\mathbf{J}\boldsymbol{L}_{\sigma}$. After Laplace transforming (42), the reduced-order stator-impedance matrix (31) is obtained.

Acknowledgment

This work was supported by the Finnish Funding Agency for Technology and Innovation, ABB Oy, Kone Oyj, and High Speed Tech Oy Ltd.

References

[1] A. Yahiaoui and F. Bouillault, "Saturation effect on the electromagnetic behaviour of an induction machine," *IEEE Trans. Magn.*, vol. 31, no. 3, pp. 2036–2039, May 1995.

[2] C. Gerada, K. J. Bradley, M. Sumner, and P. Sewell, "Evaluation and modelling of cross saturation due to leakage flux in vector controlled induction machines," *IEEE Trans. Ind. Appl*, vol. 43, no. 3, pp. 694–702, May/June 2007.

[3] M. Hinkkanen, A.-K. Repo, and J. Luomi, "Influence of magnetic saturation on induction motor model selection," in *Proc. ICEM'06*, Chania, Greece, Sept. 2006, CD-ROM.

[4] H. A. Toliyat, E. Levi, and M. Raina, "A review of RFO induction motor parameter estimation techniques," *IEEE Trans. Energy Convers.*, vol. 18, no. 2, pp. 271–283, June 2003.

[5] P. L. Jansen and R. D. Lorenz, "Transducerless field orientation concepts employing saturation-induced saliences in induction machines," *IEEE Trans. Ind. Appl.*, vol. 32, no. 6, pp. 1380–1393, Nov./Dec. 1996.

[6] F. Blaschke, J. van der Burgt, and A. Vandenput, "Sensorless direct field orientation at zero flux frequency," in *Conf. Rec. IEEE-IAS Annu. Meeting*, vol. 1, San Diego, CA, Oct. 1996, pp. 189–196.

[7] M. L. Aime, M. W. Degner, and R. D. Lorenz, "Saturation measurements in AC machines using carrier signal injection," in *Conf. Rec. IEEE-IAS Annu. Meeting*, vol. 1, St. Louis, MO, Oct. 1998, pp. 159–166.

[8] G. R. Slemon and E. A. Ismailov, "An analysis of the harmonic impedance of a saturated induction machine," *IEEE Trans. Power App. Syst.*, vol. PAS-99, no. 4, pp. 1663–1669, July 1980.

[9] J. A. A. Melkebeek, "Magnetising-field saturation and dynamic behaviour of induction machines; Part I: Improved calculation method for induction-machine dynamics," *IEE Proc. B, Electr. Power Appl.*, vol. 130, no. 1, pp. 1–9, Jan. 1983.

[10] J. A. A. Melkebeek and D. W. Novotny, "The influence of saturation on induction machine drive dynamics," *IEEE Trans. Ind. Appl.*, vol. IA-19, no. 5, pp. 671–681, Sept. 1983.

[11] L. O. Chua, "Dynamic nonlinear networks: State-of-the-art," *IEEE Trans. Circuits Syst.*, vol. CAS-27, no. 11, pp. 1059–1087, Nov. 1980.

[12] P. W. Sauer, "Constraints on saturation modeling in ac machines," *IEEE Trans. Energy Convers.*, vol. 7, no. 1, pp. 161–167, Mar. 1992.

[13] A. Arkkio, "Analysis of induction motors based on the numerical solution of the magnetic field and circuit equations," Ph.D. dissertation, Dept. Elect. Commun. Eng., Helsinki Univ. Tech., Espoo, Finland, Dec. 1987. [Online]. Available: http://lib.tkk.fi/Diss/198X/isbn951226076X/

[14] A. Repo and A. Arkkio, "Numerical impulse response test to estimate circuit-model parameters for induction machines," *IEE Proc. Electr. Power Appl.*, vol. 153, no. 6, pp. 883–890, Nov. 2006.
[15] A. Tabesh and R. Iravani, "Frequency-response analysis of torsional dynamics," *IEEE Trans. Power Syst.*, vol. 19, no. 3, pp. 1430–1437, Aug. 2004.
[16] L. Harnefors, "Analysis of subsynchronous torsional interaction with power electronic converters," *IEEE Trans. Power Syst.*, vol. 22, no. 1, pp. 305–313, Feb. 2007.
[17] D. Holliday, T. C. Green, and B. W. Williams, "On-line measurement of induction machine stator and rotor winding parameters," in *Proc. IEE PEVD Conf.*, London, U.K., Oct. 1994, pp. 465–469.
[18] M. Hinkkanen, A.-K. Repo, M. Cederholm, and J. Luomi, "Small-signal model for saturated deep-bar induction machines," in *Proc. EPE'07*, Aalborg, Denmark, Sept. 2007, CD-ROM.
[19] A.-K. Repo, P. Rasilo, A. Niemenmaa, and A. Arkkio, "Identification of electromagnetic torque model for induction machines with numerical magnetic field solution," *IEEE Trans. Magn.*, vol. 44, no. 6, pp. 1586–1589, June 2008.

Marko Hinkkanen (M'06) received the M.Sc.(Eng.) and D.Sc.(Tech.) degrees from Helsinki University of Technology, Espoo, Finland, in 2000 and 2004, respectively. Since 2000, he has been with Helsinki University of Technology. He is currently an Adjunct Professor with the Department of Electrical Engineering, Helsinki University of Technology. His research interests are in the areas of electric drives and electric machines.

Anna-Kaisa Repo received the M.Sc.(Eng.) and D.Sc.(Tech.) degrees from Helsinki University of Technology, Espoo, Finland, in 2004 and 2008, respectively. She is currently an R&D engineer with Konecranes. Her research interests are in the areas of electrical machines, control, and system identification.

Mikaela Ranta née Cederholm was born in Pedersöre, Finland, in 1981. She received her M.Sc.(Eng.) degree from Helsinki University of Technology, Espoo, Finland, in 2006. Since 2006, she has worked as a researcher at the Department of Electrical Engineering, Helsinki University of Technology. Her main research interest is the modeling of electric machines.

Jorma Luomi (M'92) is a Professor in the Department of Electrical Engineering, Helsinki University of Technology, Espoo, Finland. He joined Helsinki University of Technology in 1980, and from 1991 to 1998 he was a Professor at Chalmers University of Technology. His research interests are in the areas of electric drives, electric machines, and numerical analysis of electromagnetic fields. He received the M.Sc.(Eng.) and D.Sc.(Tech.) degrees from Helsinki University of Technology, in 1977 and 1984, respectively.